ARTICLE

Molten-salt fabrication of (N,F)-codoped single-crystal-like titania with high exposure of (001) crystal facet for highly efficient degradation of methylene blue under visible light irradiation

Zengying Zhao,[a] Mingchao Feng, and Zhijian Peng
School of Science, China University of Geosciences, Beijing 100083, China

Hongwei Huang[b]
School of Materials Science and Technology, China University of Geosciences, Beijing 100083, China

Zhanhu Guo[c]
Chemical and Biomolecular Engineering Department, University of Tennessee, Knoxville, Tennessee 37996, USA

Zhaohui Li
Geosciences Department, University of Wisconsin – Parkside, Kenosha, Wisconsin 53144, USA

(Received 8 January 2018; accepted 6 April 2018)

Single-crystal-like TiO_2 is claimed to be a very promising material among various catalysts. In this study, the (N,F)-co-doped single-crystal-like TiO_2 was prepared by a new molten mixing process in which the mixed nitrates were used both as a morphology modifier and an N-doping agent at the same time. The prepared samples also had well-developed (001) facet due to the addition of HF. The HF can also be an F doping agent to the material. The co-doping of N and F can diminish the band gap of TiO_2 from 3.05 to 2.93 eV, therefore visible light can be used effectively by the material. In addition, NO and fluorine ions existing on the surface of the sample can also help its photocatalyticity. Therefore, the photocatalytic performance of the as-prepared sample was effectively improved.

I. INTRODUCTION

Titanium dioxide (TiO_2) has now become one of the most efficient and widely used materials in the field of photocatalysis. It was found to display photocatalytic activities under ultraviolet (UV) light by Fujishima and Honda in 1972.[1] In 1976, Carey et al. began the study of photocatalytic degradation of pollutants using TiO_2 to remove chlorine from polychlorinated biphenyls under UV irradiation.[2] In 1977, Frank et al. successfully converted CN^- to OCN^- using TiO_2 as a photocatalyst.[3] Presently, photocatalytic technology has been considered as one of the most effective ways to solve the problems of energy and environmental pollution.[4,5] TiO_2 has many advantages including low cost, nontoxicity, long-term stability, and high photoactivity.[6–11] However, there are still some obstacles toward its broader applications in photocatalysis and other fields. One of the difficulties to use TiO_2 in practice is its wide band gap of about 3.2 eV, which means that it can only be activated by UV irradiation. UV light has a wave length below 380 nm making up only about 5% of the solar energy.[12,13] Therefore, it is very important to improve the visible light activity of the photocatalyst. Preparation of titania with high energy crystal facets is a very important method to increase the electron hole pair separation and the photocatalytic activity of the catalyst.[14,15] In recent years, the synthesis of photocatalytic TiO_2 with high energy (001) crystal facet has become a research hot-spot.[16–20] For example, Yang et al. in 2008, for the first time, successfully prepared anatase crystal TiO_2 with a (001) facet exposure rate of 10%.[21] After that, Yang synthesized TiO_2 with a 64% (001) facet exposure rate and the TiO_2 photocatalytic efficiency was greatly improved.[22] In 2009, Alivov et al. treated the TiO_2 nanotube array under a fluorine environment, and the (001) facet exposure rate of the sample was 60%.[23] In 2010, Liu et al. prepared nanocrystalline (001) anatase TiO_2 with 18% (001) facet exposure by the hydrothermal treatment.[24] Subsequently, the hollow spherical TiO_2 nanoparticles with 20% (001) facet exposure were synthesized by hydrothermal treatment at 180 °C.[25] Zhang et al. prepared anatase TiO_2 with 80% (001) crystalline (001) facet exposure by the hydrothermal reaction under microwave radiation.[26] Chen et al. synthesized wafer nanosheet layered spheres with (001) facet exposure of nearly 100%.[27]

On the other hand, it is also important to improve the quantum efficiency and photocatalytic activity of the material by modifying its morphology. Mesoporous

Address all correspondence to these authors.
[a]e-mail: zhaozy@cugb.edu.cn
[b]e-mail: hhw@cugb.edu.cn
[c]e-mail: zguo10@utk.edu
DOI: 10.1557/jmr.2018.106

single-crystal-like (MSCL) TiO_2 are promising materials for energy conversion or storage devices since they combine high surface area with large crystalline domain size. TiO_2 MSCL has been prepared by silica template strategies.[28,29] Recently, MSCL TiO_2 has also been prepared by a molten salt method.[30] The molten salt system is a special reaction medium in favor of controlling crystals growth and pore structure; therefore, it can directly affect intrinsic anisotropic growth due to its lower flowability and diffusivity.[31] However, there have limited research studies on the MSCL TiO_2 by using the molten salt system.[32–34]

In this study, TiO_2 with a high (001) facet exposure rate was prepared using HF as a modifier agent, which, at the same time, was also introduced as an F doping agent. Besides, to obtain the MSCL sample, molten mixed nitrates were added. The nitrates can also dope N into the sample under the same procedure. Therefore, nitrogen and fluorine co-doped single-crystal-like TiO_2 was prepared by this method. The composition, morphology, and structure of the as-prepared sample were analyzed. The photocatalytic activity of the sample was evaluated by degrading methylene blue (MB) in the visible light region. The samples by this method demonstrated high visible light photocatalytic activity compared with general TiO_2 samples which were unmodified by the procedure.

II. EXPERIMENTAL

A. Materials and methods

All chemicals used in this study were purchased from commercial sources and used without further purification. The nitrate-treated N-doped TiO_2 and N,F co-doped TiO_2 were prepared by the following process. First, 5 mL acetic acid was added to a polytetrafluoroethylene reactor. 2 mL tetrabutyl titanate was added dropwise under intense magnetic stirring; then 5 mL of 2 M urea solution or 5 mL of 2 M urea and HF solution were added. After stirring constantly for 30 min, the mixture was hydrothermally treated at 150 °C for 24 h. Finally, the sample was mixed with $NaNO_3$ and KNO_3 at a molar ratio of 5:1:1, and then calcined at 350 °C for 4 h. The prepared nitrate-treated N-doped and N,F co-doped TiO_2 samples were abbreviated as N-TiO_2 and (N,F)-TiO_2 (treated with nitrates). For comparison, N,F co-doped TiO_2 samples without mixing with nitrates were also prepared, which were named (N,F)-TiO_2. And the samples without urea and nitrate treating were named as pure TiO_2.

B. Characterization

The crystal phase of the samples was identified by X-ray diffraction (XRD; Rigaku D/max, Rigaku Corporation, Tokyo, Japan) scanned in the 2θ range of 20–80° at a scanning rate of 4°/min using Cu K_α radiation. The specific surface area, pore size, and pore volume of the samples were evaluated with a surface area analyzer (AutosorbiQ Station-I, Quantachrome Instruments, Boynton Beach, FL) from N_2 adsorption isotherms using the Brunauer–Emmett–Teller (BET) method. The mesopore size distribution and mesopore volume were calculated by desorption isotherms. The elemental composition of the samples was measured by X-ray photoelectron spectroscopy (XPS; ESCALAB 250) with a photon energy of 1253.6 eV and with Mg K_α radiation as the exciting source. All the binding energies were referenced to the C 1*s* peak for calibration. The crystal size and morphology of the samples were obtained by scanning electron microscopy (SEM; JEOL S-500, JEOL Ltd., Tokyo, Japan). The as-prepared samples were ground in a mortar for over 10 min. Ethanol solutions of the samples were treated by using an ultrasonic cleaner (JP-020S, JIEMENG Ltd., Shenzhen, China) for over 2 h. Several drops of the ethanol solution were dripped onto the copper wire meshes. After over 24 h of air drying, the meshes were examined by transmission electron microscopy (TEM) and high resolution transmission electron microscopy (HRTEM) (JEOL JEM-2100F, JEOL Ltd., Tokyo, Japan). The UV-Vis absorption spectra of the samples were recorded on a UV-vis scanning spectrophotometer (Perkin-Elmer, Lambda 900, Boynton Beach, FL) in the range of 200–800 nm equipped with an integrated sphere with barium sulfate ($BaSO_4$) as the reference. The band gap energy was estimated by extrapolating the linear part of the $(Ahv)^{1/2}$ versus hv curve to the energy axis.

C. Evaluation of photocatalytic activity

The photocatalytic performance of the samples was tested under visible light irradiation by decomposition of MB in aqueous media (5 mg/L). The experiment with the liquid photocatalytic reaction was carried out in the reaction test tubes that were located axially in a ring whirligig test tube rack (XPA-7, Xujiang Ltd., Nanjing, China). A xenon lamp (Lap Pu, XQ) of 500 W with a 420 nm cut-off filter right above the reactor was used as the light source to provide only visible light in the center. In each 50 mL 5 mg/L MB aqueous solution, 0.05 g photocatalysts were added.[35] Before photoreaction, the suspension was treated with ultrasound and stirred in the dark for about 30 min to reach the adsorption–desorption equilibrium between photocatalysts and MB. During the degradation process, the suspension in the test tube under the visible light irradiation was stirred by magnetic force. For every 30 min of interval, the supernatant liquid was sampled out and centrifuged to remove the photocatalysts from the suspension. The resultant transparent solutions were examined by UV/vis spectroscopy (722 s) at 662 nm to obtain the absorbance of the MB solution.

III. RESULTS AND DISCUSSION

A. Composition analysis

Figure 1 shows typical XRD patterns of pure TiO_2, N-TiO_2 (treated with nitrates), (N,F)-TiO_2, and (N,F)-TiO_2 (treated with nitrates) samples. All the samples are observed to have obvious diffraction peaks at 2θ = 25.30, 37.87, and 48.18°, which correspond to the (101), (004), and (200) facets of the anatase (JCPDS card No. 21-1272).[36,37] All the diffraction peaks of pure TiO_2, N-TiO_2 (treated with nitrates), (N,F)-TiO_2, and (N,F)-TiO_2 (treated with nitrates) samples can be indexed to the unique anatase phase, indicating that the doping with nitrogen or nitrogen and fluorine into TiO_2 would not produce any new phases.[38] Furthermore, there are no nitrogen-originated XRD peaks located in the samples, which is probably due to the low dopant content in the samples below the detection limit of the XRD test. Besides, it may also because the dopants are dispersed in the lattice of TiO_2.[39,40]

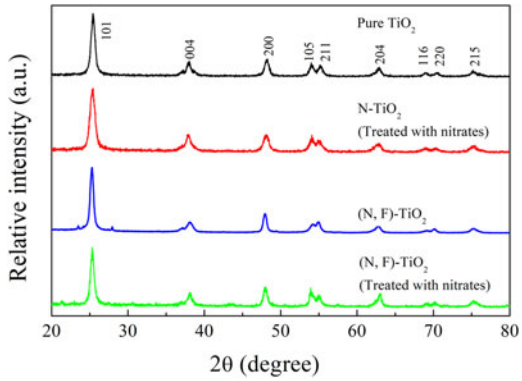

FIG. 1. Typical XRD patterns of pure TiO_2, N-TiO_2 (treated with nitrates), (N,F)-TiO_2, and (N,F)-TiO_2 (treated with nitrates) samples.

The chemical compositions of the samples were analyzed by the XPS test. Figure 2(a) shows the XPS of the (N,F)-TiO_2 (treated with nitrates) sample. The elements Ti, N, F, and O are present in the sample, corresponding to the peak of Ti 2*p* (458.5 eV), N 1*s* (400 eV), F 1*s* (684.6 eV), and O 1*s* (529.9 eV). The peak of C 1*s* (284.6 eV) is the XPS spectral icon quasi peak. The results show that TiO_2 doped with nitrogen and fluorine is successfully synthesized in this experiment.

Figure 2(b) shows the XPS spectrum of the sample in the Ti 2*p* region. The spectra of Ti 2*p* show two main peaks, which are located at 458.5 and 464.3 eV. They are attributed to the Ti $2p_{3/2}$ and Ti $2p_{1/2}$ species, respectively. And the peak is symmetrical, thus it can be determined that the Ti elements mainly exist in the form of Ti^{4+} (TiO_2).[41]

Figure 2(c) shows the O 1*s* spectrum of the sample. The peak of the binding energy is 529.9 eV, which represents the O–Ti–O bond, and it can be determined that the O elements exist mainly in the form of O^{2-}.[42] The XPS of the (N,F)-TiO_2 (treated with nitrates) sample in the N 1s region is shown in Fig. 2(d). The peak present at 400 eV indicates that nitrogen is successfully incorporated into TiO_2. This N 1*s* peak can also be

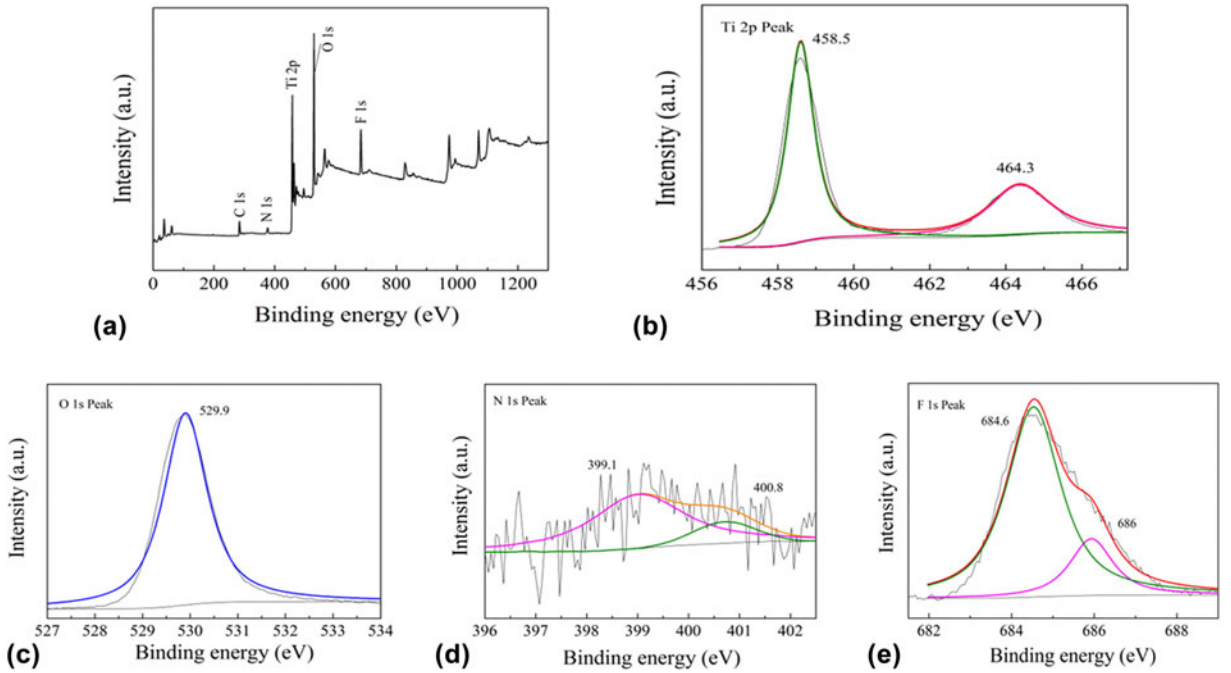

FIG. 2. Typical XPS results of the (N,F)-TiO_2 (treated with nitrates) sample: (a) survey spectrum, (b) Ti 2*p* peaks, (c) O 1*s* peaks, (d) N 1*s* peaks, and (e) F 1*s* peaks.

separated into two peaks. The peak at 399.1 eV can be attributed to the N existed in the form of O–Ti–N. The other peak located at 400.8 eV can be attributed to the N in the bond of N–O, which may be the NO adsorbed on the surface of the sample and/or in the bond of Ti–O–N.[43] Because the NO has strong oxidizability, it is very favorable for the photocatalytic reaction.

Figure 2(e) shows the XPS spectrum of the sample in the F 1*s* region. The peak appears to be around 684.6 eV. This F 1*s* peak can be separated into two peaks located at 686 eV and 684.6 eV, respectively. The peak at 686 eV can be attributed to the F in the form of Ti–F in the TiO_2. This result shows that the F is incorporated into the TiO_2 lattice. The other peak located at 684.6 eV can be attributed to the F ions that adsorbed on the surface of TiO_2.[44] This form of F ions can react with OH^- in water to form hydroxyl radicals. And the catalytic activity of a hydroxyl radical in the aqueous solution is higher than that on the surface of the catalyst. Therefore, it can degrade organic dyes in aqueous solution more quickly.

B. Morphological structure

Figure 3 shows the SEM morphology of the samples. As can be seen from Fig. 3(a), pure TiO_2 is composed of uneven sized particles with grain size often over 10 μm. The size of other three TiO_2 samples is obviously much small in the grain size as shown in Figs. 3(b)–3(d). Therefore, small irregular grains are observed to adhere onto the large particles with the particle size ranging from a few nanometers to a few microns. It can be concluded that nitrogen doping may lead to grain refinement and agglomeration reduction.[45]

Figure 4 shows the morphology of TiO_2 samples. From Figs. 4(a)–4(c), these sample grains are small particles that are attached together. N-TiO_2 (treated with nitrates) and (N,F)-TiO_2 samples are irregular nanocrystals, while (N,F)-TiO_2 (treated with nitrates) exhibits cubic crystalline grains. According to the particle size distribution (Fig. S1), it is estimated that the average particle size of N-TiO_2 (treated with nitrates) is about 7 nm, while the diameter of (N,F)-TiO_2 (treated with nitrates) is about 13 nm. Fluorine doping enlarged the particle grain to some extent. The reason may be related to the energetic surfaces of the crystal sample caused by the HF.[46,47]

From HRTEM micrographs of Fig. 4(d), it is clear that (N,F)-TiO_2 (treated with nitrates) is a nanocubic block. The crystalline spacing of the sample is 0.235 nm, which matches the anatase phase TiO_2 (001) surface.[48,49] But in the XRD test, according to the extinction rule, there is no (001) diffraction peak. The high energy (001) surface is exposed by the synergistic effects of molten salt and the etching of HF. Due to the low fluidity and diffusivity of mixed nitrates, relatively slow nucleation and growth rates can be induced, thus the grain growth is suppressed.

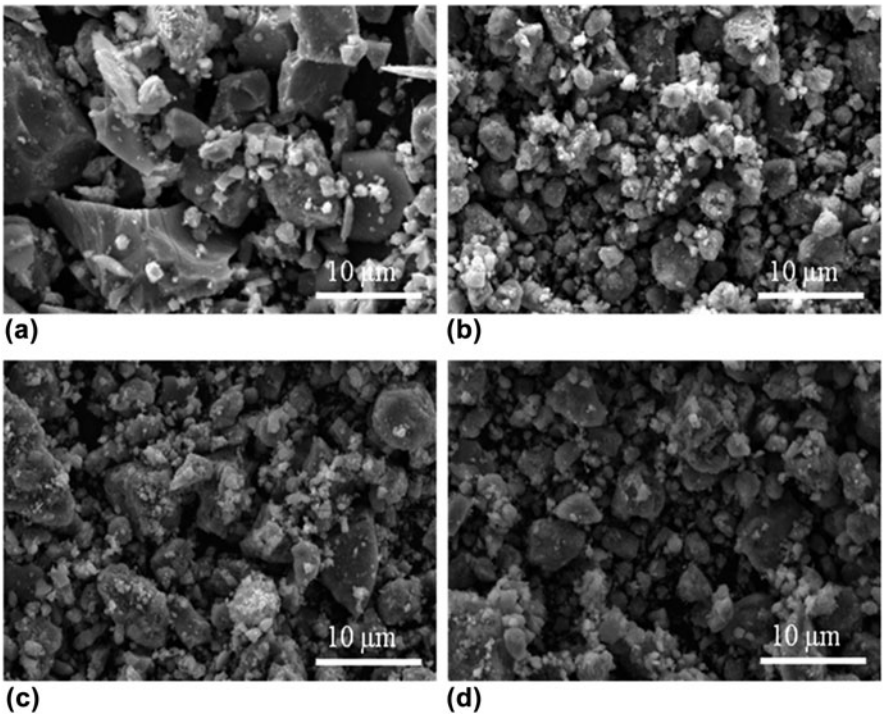

FIG. 3. Typical SEM images of (a) pure TiO_2, (b) N-TiO_2 (treated with nitrates), (c) (N,F)-TiO_2, and (d) (N,F)-TiO_2 (treated with nitrates) samples.

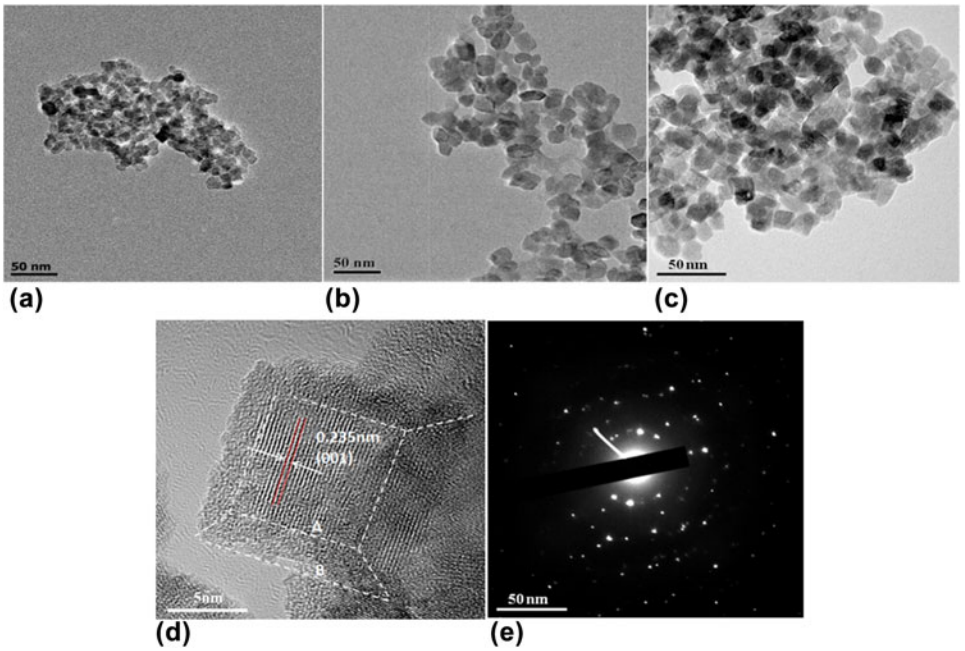

FIG. 4. TEM (a–c) of N-TiO_2 (treated with nitrates), (N,F)-TiO_2, and (N,F)-TiO_2 (treated with nitrates) samples, HRTEM (d) and SAED (e) images of the (N,F)-TiO_2 (treated with nitrates) sample.

TiO_2 can be modified by F to expose the high-energy surface of TiO_2 under relatively stable conditions.[50,51]

However, the exposure of energetic surfaces may also promote the growth of grains. Therefore, the average diameter of (N,F)-TiO_2 (treated with nitrates) is greater than that of N-TiO_2 (treated with nitrates). While the grain of the (N,F)-TiO_2 samples without nitrate treating grow larger during calcination. According to the symmetries of anatase TiO_2, the two square surfaces in the crystal of the (N,F)-TiO_2 (treated with nitrates) sample can be assigned to the (001) facet, and the eight isosceles trapezoidal surfaces are (101) facets. On the basis of the shape-dependent thermodynamic model, the value of B/A [the length parameters illustrated in Fig. 4(d)] and the percentage of (001) facet can be roughly predicted.[52] The calculation of the exposure rate of the TiO_2 energetic surfaces has been reported in the literature.[53–55] In this experiment, according to this method, the high energy surface exposure rate of the (N,F)-TiO_2 (treated with nitrates) sample was as high as 78%. The exposed (001) energetic surface can produce more electron hole pairs. Hydroxyl radicals are produced in the condition of oxides in aqueous solution and the (001) high energetic surface. The produced hydroxyl radicals can effectively improve the photocatalytic activity to degrade organic dyes in solution. Additionally, from the electron diffraction pattern of the (N,F)-TiO_2 (treated with nitrates) sample in Fig. 4(e), we can see that the sample is of a single crystal structure. Besides, as discussed above, because the formation of the (001) high energetic facet, the crystal particle tends to grow larger to reduce its surface energy. Therefore the sample (N,F)-TiO_2 (treated with nitrates) has larger particle size than the N-TiO_2 (treated with nitrates). This is consistent with the crystal particle test as shown in Fig. 4 and the discussion above that fluorine doping can enlarge the particle grain to some extent.

The recorded N_2 adsorption–desorption isotherms for the samples show that the pure TiO_2, N-TiO_2 (treated with nitrates) and (N,F)-TiO_2 samples belong to the type IV with the H2 hysteresis loop, indicating the existence of the mesoporous structure according to the IUPAC classification (Fig. S2). The formation of the mesoporous structure is probably due to the shrinking of crystals at high temperatures, which leaves space in the crystals.[56] However, the (N,F)-TiO_2 (treated with nitrates) sample belongs to the type IV with the H4 hysteresis loop. This indicates that the mesoporous structure of the samples is formed by the accumulation of the mesopores and the cubic crystalline grains existed in the sample.[57,58]

According to the measured results by the BET method, the specific surface area, pore size, and pore volume of the samples were calculated. The results are listed in Table I. The specific surface area of the (N,F)-TiO_2 is the minimum of the three samples (79.6 m^2/g), followed by the (N,F)-TiO_2 (treated with nitrates) (81.4 m^2/g), and the sample N-TiO_2 (treated with nitrates) has the maximum specific surface area, which is up to 150.6 m^2/g. The small specific surface area of the (N,F)-TiO_2 (treated with nitrates) may be due to the high energy exposure which can promote the grain growth. And for the (N,F)-TiO_2 samples, the calcination without the nitrates can induce the grain growth, resulting in the decrease of its specific area.

C. Photocatalytic properties

Figure 5(a) shows the UV-Vis absorption spectra of the samples, which include pure TiO_2, N-TiO_2 (treated with nitrates), (N,F)-TiO_2, and (N,F)-TiO_2 (treated with nitrates). The light absorption of pure TiO_2 is limited to the UV region, while the absorption wavelengths of (N,F)-TiO_2 and (N,F)-TiO_2 (treated with nitrates) extend from 380 to 600 nm. The N and F co-doping results in a red shift compared with that of the pure TiO_2. Moreover, the absorption capacity of the three N and F co-doped samples to the visible light was remarkably improved. Among them, the (N,F)-TiO_2 (treated with nitrates) sample has the most obvious increase in the light absorption capacity in the visible region. This may be due to the incorporation of nitrogen into TiO_2 as shown and discussed in Fig. 2(d). It is speculated that the N 2*p* and O 2*p* orbitals may hybridize and new impurity energy level may generate over the TiO_2 valence band.[59,60] Analogously, when F is doped into TiO_2, there may also form an impurity energy level below the TiO_2 conduction band.[61–63] This impurity energy level can reduce the band gap and the energy needed to excite the electron transition. In this case, the visible light may be able to provide sufficient energy for the electron transition. As a result, the utilization of the sample (N,F)-TiO_2 (treated with nitrates) to visible light can be improved, and its photocatalytic reaction can also be promoted.

TABLE I. Structural properties of pure TiO_2, N-TiO_2 (treated with nitrates), (N,F)-TiO_2, and (N,F)-TiO_2 (treated with nitrates) samples.

Sample	S_{BET}[a] (m^2/g)	PV[b] (cm^3)	PD[c] (nm)
Pure TiO_2	107.2	2.078	7.7
N-TiO_2 (treated with nitrates)	150.6	1.219	3.2
(N,F)-TiO_2	79.6	2.293	4.6
(N,F)-TiO_2 (treated with nitrates)	81.4	2.098	5.2

[a]The specific surface area was calculated using BET equation.
[b]Pore volume.
[c]Pore diameter.

Figure 5(b) shows the Kubelka–Munk curves of the samples obtained via the transformation based on the $(Ahv)^{1/2}$ versus energy of the absorbed light. The band gap values of the pure TiO_2, N-TiO_2 (treated with nitrates), (N,F)-TiO_2, and (N,F)-TiO_2 (treated with nitrates) samples are estimated by the Kubelka–Munk curves as shown in Table II. They are 3.05, 3.01, 2.98, and 2.93 eV, respectively. There into, the band gap value of the (N,F)-TiO_2 (treated with nitrates) sample is the highest. It is consistent with the fact shown in Fig. 5(a) that there is an obvious red shift for the (N,F)-TiO_2 (treated with nitrates) sample and its visible light absorption has remarkably improved.

The photocatalytic activities of the pure TiO_2, N-TiO_2 (treated with nitrates), (N,F)-TiO_2, and (N,F)-TiO_2 (treated with nitrates) samples are evaluated by the degradation of MB versus irradiation time under visible light. The results are shown in Fig. 6(a). A blank sample was used as a control. The decolorization rate of MB without the catalyst is 10% after 150 min of irradiation time. The decolorization rate of MB with the (N,F)-TiO_2 (treated with nitrates) sample is 89%, and it is the highest among the several samples. Under the same conditions, decolorization rate is 73 and 60% for the N-TiO_2 (treated with nitrates) and the (N,F)-TiO_2 samples, respectively, while the pure TiO_2 has almost no catalytic activity in visible light region. The linear relationship between the reaction time and $-\ln(C/C_0)$ is shown in Fig. 6(b). The figure indicates that the degradation of MB follows the first-order kinetics. The rate constants of the pure TiO_2, N-TiO_2 (treated with nitrates), (N,F)-TiO_2, and (N,F)-TiO_2 (treated with nitrates) samples are estimated to be 0.00022, 0.0052, 0.0046, and 0.013 min^{-1}, respectively. The maximum rate constant of the sample (N,F)-TiO_2 (treated with nitrates) shows that it has best photocatalytic performance.[52,64–67] To demonstrate the stability of catalysts, the catalytic activity of (N,F)-TiO_2 (treated with nitrates) has been performed five runs under the same conditions after centrifugal separations. The results

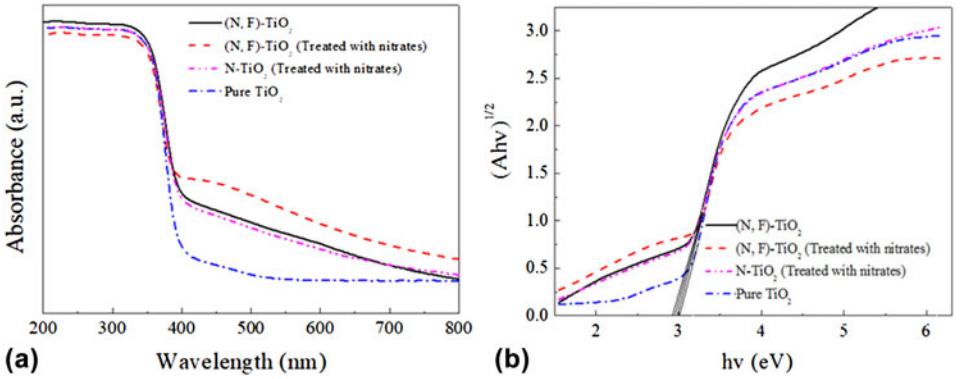

FIG. 5. (a) UV-Vis absorption spectra of the pure TiO_2, N-TiO_2 (treated with nitrates), (N,F)-TiO_2, and (N,F)-TiO_2 (treated with nitrates) samples, and (b) their corresponding Kubelka–Munk curves.

illustrate that the MB degradation rate only slightly decreases after repeated irradiation for near 800 min, which indicates sufficient stability of the present photocatalyst for MB degradation (Fig. S3).

As the electrochemical impedance spectra (EIS) Nyquist plots are supposed to indicate the charge separation and transfer process in the electrode−electrolyte interface region,[68] the EIS technology was used to study the photocatalytic performance.[69] Figure 7 shows Nyquist plots of the as-prepared samples before and after visible light irradiation. It can be observed that the arc radius of (N,F)-TiO_2 (treated with nitrates) is the smallest one, which indicates that this sample exhibits a higher separation and transfer efficiency of photogenerated e–h pairs.[70–72]

The investigation of the reactive oxidation species in the photocatalytic process is very important to the explication of the photocatalytic mechanism. To trap the reactive oxidation species in experiments, under the same experiment condition for each photocatalytic test on MB by (N,F)-TiO_2 (treated with nitrates), 1 mM TBA and BQ, as scavengers of hydroxyl radicals ($^{\cdot}OH$) and superoxide radicals ($^{\cdot}O^{2-}$), were added into the reaction system, respectively.[31] Figure S4 shows the degradation curves of MB by the catalysis of (N,F)-TiO_2 (treated with nitrates) in the presence of scavengers under visible light irradiation. It can be seen that the photocatalytic efficiency was both decreased. There into, the TBA is of higher inhibition efficiency for degradation of MB (54.8%). Thus, it could be speculated that $^{\cdot}OH$ serves as the main reactive oxidation species for the photodegradation of MB under sunlight irradiation.

Based on the above experimental results and discussion, the possible photocatalysis mechanism is illustrated in Fig. 8. The gradient in the energy band represents the mixing of the N 2*p* and O 2*p* atomic orbitals.[51,52] The nitrogen doping in the TiO_2 lattice can create an intraband-gap state (N 2*p*), which are located above the valence band edge (O 2*p*). Thus, the electron-excited driving force by the N 2*p* level is increased. On the other hand, the (N,F)-doped sample has a better photocatalytic performance than the N-doped sample. The possible

TABLE II. Band gap energy (E_g) of pure TiO_2, N-TiO_2 (treated with nitrates), (N,F)-TiO_2, and (N,F)-TiO_2 (treated with nitrates) samples.

Sample	Pure TiO_2	N-TiO_2 (treated with nitrates)	(N,F)-TiO_2	(N,F)-TiO_2 (treated with nitrates)
E_g (eV)	3.05	3.01	2.98	2.93

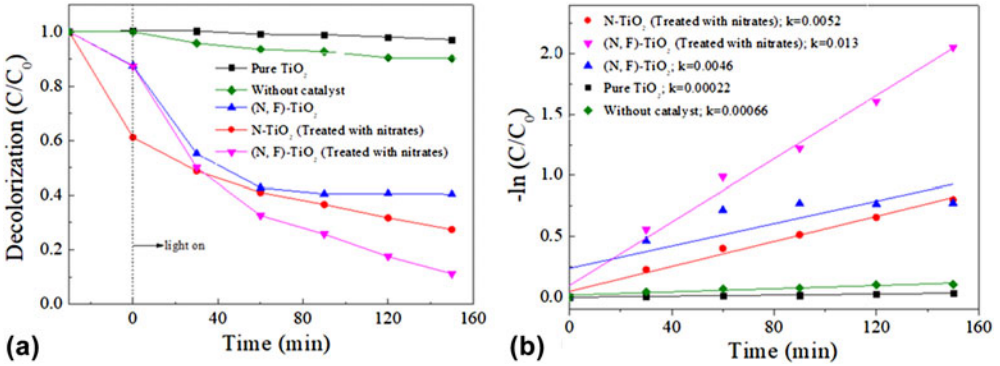

FIG. 6. (a) Degradation curves of MB by the catalysis of pure TiO_2, N-TiO_2 (treated with nitrates), (N,F)-TiO_2, and (N,F)-TiO_2 (treated with nitrates) samples under visible light irradiation, and (b) their corresponding plots of $-\ln(C/C_0)$.

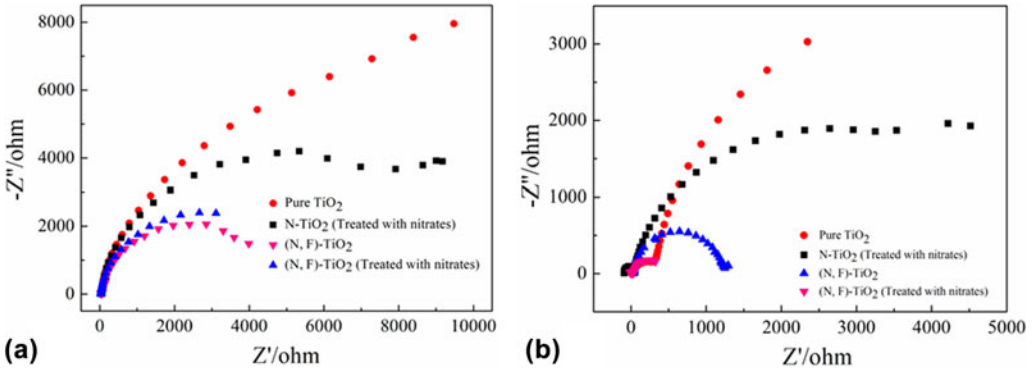

FIG. 7. EIS Nyquist plots of the samples with (a) light off/(b) light on cycles under the irradiation of visible light (A xenon lamp with a cut-off filter $\lambda \geq 420$ nm, $[Na_2SO_4] = 0.1$ M).

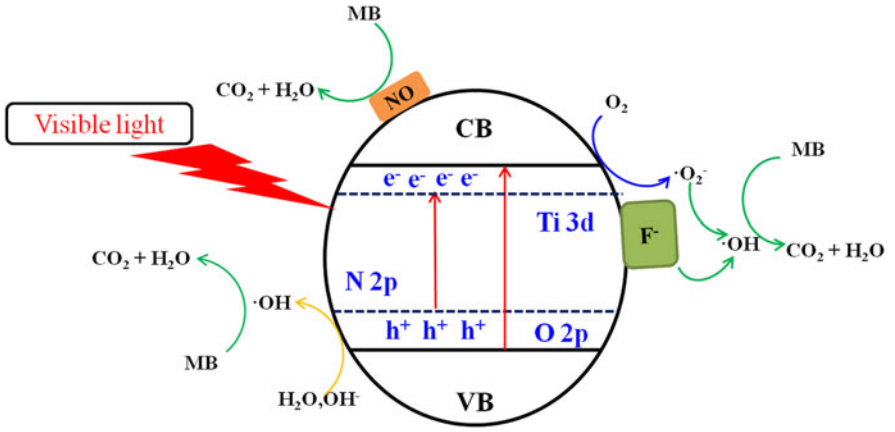

FIG. 8. Mechanism for photocatalytic degradation of MB over (N,F)-TiO_2 (treated with nitrates) photocatalysts under visible light irradiation.

explanation is that a Ti–F bond is formed in the sample, and an impurity energy level is also formed below the TiO_2 conduction band.[69,73]

The F ion has a strong electronegativity so that the Ti–F groups on the surface can act as the electron capture sites. These electron capture sites can trap the excited electrons and reduce the absorbed O_2 to superoxide radicals O_2^- [seen in the Eq. (2)], thereby reducing the recombination of electrons and holes.[74,75]

The major reactions in this photocatalytic mechanism are summarized by the following steps:

$$(\mathrm{N,F})\text{-}\mathrm{TiO_2}(\text{treated with nitrates}) + \text{visible light} \rightarrow (\mathrm{N,F})\text{-}\mathrm{TiO_2}(\text{treated with nitrates})(\mathrm{e^- + h^+}) \quad , \tag{1}$$

$$\mathrm{O_2 + e^- \rightarrow {}^{\bullet}O_2^-} \quad , \tag{2}$$

$$\mathrm{{}^{\bullet}O_2^- + H^+ + e^- \rightarrow {}^{\bullet}OH + OH^-} \quad , \tag{3}$$

$$\mathrm{OH^- + h^+ \rightarrow {}^{\bullet}OH} \quad , \tag{4}$$

$$\mathrm{{}^{\bullet}OH + MB \rightarrow degradation} \quad , \tag{5}$$

and

$$\mathrm{NO + MB \rightarrow degradation} \quad . \tag{6}$$

IV. CONCLUSIONS

In this study, (N,F)-co-doped MSCL TiO_2 was prepared by a new molten salt method. The molten nitrates can be used as the morphology modifier in the formation of the MSCL TiO_2, and it can also be used as an N doping agent in the same process. This material also has a high (001) surface exposure rate of 78%, meanwhile HF is used as the (001) crystal facet modifier and also used as an F doping agent. The exposed high energy crystal facet can produce more electron hole pairs; therefore, it can effectively improve the photocatalytic activity of the catalyst. The N and F co-doping can reduce the band gap of the as-prepared sample from 3.05 to 2.93 eV and then improve its utilization of the visible light. In addition, the presence of NO and fluorine ions on the surface of the sample can also help to enhance the photocatalytic performance. Therefore, the (N,F)-TiO_2 (treated with nitrates) has the best photocatalytic ability among the samples of pure TiO_2, (N,F)-TiO_2, and N-TiO_2 (treated with nitrates).

ACKNOWLEDGMENTS

This project is financially supported by the Fundamental Research Funds for the Central Universities of China No. 2652017150, and the innovative experiment projects of China University of Geosciences (Beijing) Nos. 2017BXY033 and 2017BXY034.

REFERENCES

1. A. Fujishima and K. Honda: Electrochemical photocatalysis of water at semiconductor electrode. *Nature* **238**, 37–38 (1972).
2. J.H. Carey, J. Lawrence, and H.M. Tosine: Photodechlorination of PCB'S in the presence of titanium dioxide in aqueous suspensions. *Bull. Environ. Contam. Toxicol.* **16**, 697 (1976).
3. S.N. Frank and A.J. Bard: Heterogeneous photocatalytic oxidation of cyanide and sulfite in aqueous solutions at semiconductor powders. *J. Phys. Chem.* **81**, 1484 (1977).
4. E. Perez, L. Vittorio, M.F. Torres, E. Sham, and E. Pérez: Nitrogen doped TiO_2 photoactive in visible light. *Mater.-Rio De Janeiro* **20**, 561 (2015).
5. A. Primo and H. Garcia: Solar photocatalysis for environment remediation. *New Future Dev. Catal.* **6**, 145 (2013).
6. A. Fujishima and X. Zhang: Titanium dioxide photocatalysis: Present situation and future approaches. *C. R. Chim.* **9**, 750 (2006).
7. A. Fujishima, T.N. Rao, and D.A. Tryk: Titanium dioxide photocatalysis. *J. Photochem. Photobiol. Chem.* **1**, 1 (2000).

8. O.K. Varghese, M. Paulose, T.J. La Tempa, and C.A. Grimes: High-rate solar photocatalytic conversion of CO_2 and water vapor to hydrocarbon fuels. *Nano Lett.* **9**, 731 (2009).
9. J. Yu, Y. Wang, and W. Xiao: Enhanced photoelectrocatalytic performance of SnO_2/TiO_2 rutile composite films. *J. Mater. Chem. A* **1**, 10727 (2013).
10. J. Yang, X. Zhang, B. Li, H. Liu, P. Sun, C. Wang, L. Wang, and Y. Liu: Photocatalytic activities of heterostructured TiO_2-graphene porous microspheres prepared by ultrasonic spray pyrolysis. *J. Alloys Compd.* **584**, 180 (2014).
11. B. Qiu, M. Xing, and J. Zhang: Mesoporous TiO_2 nanocrystals grown in situ on graphene aerogels for high photocatalysis and lithium-ion batteries. *J. Am. Chem. Soc.* **136**, 5852 (2014).
12. C. Burda, Y. Lou, X. Chen, A.C.S. Samia, J. Stout, and J. Gole: Enhanced nitrogen doping in TiO_2 nanoparticles. *Nano Lett.* **3**, 1049 (2003).
13. H.W. Huang, X.W. Li, J. Wang, F. Dong, P.K. Chu, T. Zhang, and Y.H. Zhang: Anionic group self-doping as a promising strategy: Band-gap engineering and multi-functional applications of high-performance CO_{32}-doped $Bi_2O_2CO_3$. *ACS Catal.* **5**, 4094 (2015).
14. Z. Mesgari and J. Saien: Pollutant degradation over dye sensitized nitrogen doped titanium substances in different configurations of visible light helical flow photoreactor. *Sep. Purif. Technol.* **185**, 129 (2017).
15. Q.J. Xiang, J.G. Yu, and M. Jaroniec: Tunable photocatalytic selectivity of TiO_2 films consisted of flower-like microspheres with exposed {001} facets. *Chem. Commun.* **47**, 4532 (2011).
16. Z.C. Lai, F. Peng, Y. Wang, H. Wang, H. Yu, P. Liub, and H. Zhao: Low temperature solvothermal synthesis of anatase TiO_2 single crystals with wholly {100} and {001} faceted surfaces. *J. Mater. Chem.* **22**, 23906 (2012).
17. L. Sun, Z. Zhao, Y. Zhou, and L. Liu: Anatase TiO_2 nanocrystals with exposed {001} facets on graphene sheets via molecular grafting for enhanced photocatalytic activity. *Nanoscale* **4**, 613 (2012).
18. J. Zhang, L. Zhang, Y. Shi, G. Xu, E. Zhang, H. Wang, Z. Kong, J. Xi, and Z. Ji: Anatase TiO_2 nanosheets with coexposed {101} and {001} facets coupled with ultrathin SnS_2 nanosheets as a face-to-face n–p–n dual heterojunction photocatalyst for enhancing photocatalytic activity. *Appl. Surf. Sci.* **420**, 839 (2017).
19. Y. Cao, L. Zong, Q. Li, C. Li, J. Li, and J. Yang: Solvothermal synthesis of TiO_2 nanocrystals with {001} facets using titanic acid nanobelts for superior photocatalytic activity. *Appl. Surf. Sci.* **391**, 311 (2017).
20. D. Li, F. Chen, D. Jiang, W. Shi, and W. Zheng: Enhanced photocatalytic activity of N-doped TiO_2 nanocrystals with exposed {001} facets. *Appl. Surf. Sci.* **390**, 689 (2016).
21. H.G. Yang, C.H. Sun, S.Z. Qiao, J. Zou, G. Liu, S.C. Smith, H.M. Cheng, and G.Q. Lu: Anatase TiO_2 single crystals with a large percentage of reactive facets. *Nature* **453**, 638 (2008).
22. H.G. Yang, G. Liu, S.Z. Qiao, C.H. Sun, Y.G. Jin, S.C. Smith, J. Zou, H.M. Cheng, and G.Q. Lu: Solvothermal synthesis and photoreactivity of anatase TiO_2 nanosheets with dominant {001} faces. *J. Am. Chem. Soc.* **131**, 4078 (2009).
23. Y. Alivov and Z.Y. Fan: A method for fabrication of pyramid-shaped TiO_2 nanoparticles with a high {001} facet percentage. *J. Phys. Chem. C* **113**, 12954 (2009).
24. G. Liu, C.H. Sun, H.G. Yang, S.C. Smith, L. Wang, G.Q. Lu, and H.M. Cheng: Nanosized anatase TiO_2 single crystals for enhanced photocatalytic activity. *Chem. Commun.* **46**, 755 (2010).
25. S.W. Liu, G.Y. Yu, and M. Jaroniec: Tunable photocatalytic selectivity of hollow TiO_2 microspheres composed of anatasepolyhedra with exposed {001} facets. *J. Am. Chem. Soc.* **132**, 11914 (2010).
26. Q.F. Zhang, C.S. Dandeneau, X.Y. Zhou, and G.Z. Cao: ZnO nanostructures for dye-sensitized solar cells. *Adv. Mater.* **21**, 4087 (2009).
27. J.S. Chen, Y.L. Tan, C.M. Li, Y.L. Cheah, D. Luan, S. Madhavi, F.Y. Boey, L.A. Archer, and X.W. Lou: Constructing hierarchical spheres from large ultrathin anatase TiO_2 nanosheets with nearly 100% exposed (001) facets for fast reversible lithium storage. *J. Am. Chem. Soc.* **132**, 6124 (2010).
28. X. Zheng, Q. Kuang, K. Yan, Y. Qiu, J. Qiu, and S. Yang: Mesoporous TiO_2 single crystals: Facile shape-, size-, and phase-controlled growth and efficient photocatalytic performance. *ACS Appl. Mater. Interfaces* **5**, 11249 (2013).
29. V. Sivaram, E.J.W. Crossland, T. Leijtens, N.K. Noel, J. Alexander-Webber, P. Docampo, and H.J. Snaith: Observation of annealing-induced doping in TiO_2 mesoporous single crystals for use in solid state dye sensitized solar cells. *J. Phys. Chem. C* **118**, 1821 (2014).
30. C. Li, G. Chen, J. Sun, J. Rao, Z. Han, Y. Hu, and Y. Zhou: A novel mesoporous single-crystal-like Bi_2WO_6 with enhanced photocatalytic activity for pollutants degradation and oxygen production. *ACS Appl. Mater. Interfaces* **7**, 25716 (2015).
31. C.X. Li, Z.Y. Zhao, H.S. Lomboleni, H.W. Huang, and Z.J. Peng: Enhanced visible photocatalytic activity of nitrogen doped single crystal-like TiO_2 by synergistic treatment with urea and mixed nitrates. *J. Mater. Res.* **32**, 737 (2017).
32. H. Yu, R. Shi, Y. Zhao, T. Bian, Y. Zhao, C. Zhou, G.I.N. Waterhouse, L. Wu, C. Tung, and T. Zhang: Alkali-assisted synthesis of nitrogen deficient graphitic carbon nitride with tunable band structures for efficient visible-light-driven hydrogen evolution. *Adv. Mater.* **29**, 1605148–1605156 (2017).
33. Y. Zhao, B. Zhao, J. Liu, G. Chen, R. Gao, S. Yao, M. Li, Q. Zhang, L. Gu, J. Xie, X. Wen, L. Wu, C. Tung, D. Ma, and T. Zhang: Oxide-modified nickel photocatalysts for the production of hydrocarbons in visible light. *Angew. Chem. Int. Ed.* **55**, 4215 (2016).
34. Y. Zhao, G. Chen, T. Bian, C. Zhou, G.I.N. Waterhouse, L. Wu, C. Tung, L.J. Smith, D. O'Hare, and T. Zhang: Defect-rich ultrathin znal-layered double hydroxide nanosheets for efficient photoreduction of CO_2 to CO with water. *Adv. Mater.* **27**, 7824 (2015).
35. L. Zheng, X. Yu, M. Long, and Q. Li: Humic acid-mediated visible-light degradation of phenol on phosphate-modified and Nafion-modified TiO_2 surfaces. *Chin. J. Catal.* **38**, 2076 (2017).
36. H.W. Huang, K. Xiao, Y. He, T. Zhang, F. Dong, X. Du, and Y.H. Zhang: In situ assembly of BiOI@$Bi1_2O_{17}C_{l2}$ p–n junction: Charge induced unique front-lateral surfaces coupling heterostructure with high exposure of BiOI {001} active facets for robust and nonselective photocatalysis. *Appl. Catal. B Environ.* **199**, 75 (2016).
37. H.W. Huang, Y. He, X. Li, M. Li, C. Zeng, F. Dong, X. Du, T. Zhang, and Y.H. Zhang: $Bi_2O_2(OH)(NO_3)$ as a desirable $[Bi_2O_2]^{(2+)}$ layered photocatalyst: Strong intrinsic polarity, rational band structure and {001} active facets co-beneficial for robust photooxidation capability. *J. Mater. Chem. A* **3**, 24547 (2015).
38. Z. Lyu, B. Liu, R. Wang, and L. Tian: Synergy of palladium species and hydrogenation for enhanced photocatalytic activity of {001} facets dominant TiO_2 nanosheets. *J. Mater. Res.* **32**, 2781 (2017).
39. X. Cheng, X. Yu, Z. Xing, and L. Yang: Enhanced visible light photocatalytic activity of mesoporous anatase TiO_2 codoped with nitrogen and chlorine. *Int. J. Photoenergy* **2012**, 1 (2012).

40. X. Wang, S. Shen, Z. Feng, and C. Li: Time-resolved photoluminescence of anatase/rutile TiO_2 phase junction revealing charge separation dynamics. *Chin. J. Catal.* **37**, 2059 (2016).
41. S.K. Kassahun, Z. Kiflie, D.W. Shin, S.S. Park, W.Y. Jung, and Y.R. Chung: Facile low temperature immobilization of N-doped TiO_2 prepared by sol–gel method. *J. Sol-Gel Sci. Technol.* **83**, 698 (2017).
42. T.C. Jagadale, S.P. Takale, R.S. Sonawane, H.M. Joshi, S.I. Patil, B.B. Kale, and S.B. Ogale: N-doped TiO_2 nanoparticle based visible light photocatalyst by modified peroxide sol–gel method. *J. Phys. Chem. C* **112**, 14595 (2008).
43. B. Naik, S.Y. Moon, S.H. Kim, and J.Y. Park: Enhanced photocatalytic generation of hydrogen by Pt-deposited nitrogen-doped TiO_2 hierarchical nanostructures. *Appl. Surf. Sci.* **354**, 347 (2015).
44. M.S. Jyothi, P.D. Souza Laveena, R. Shwetharani, and G.R. Balakrishna: Novel hydrothermal method for effective doping of N and F into nano titania for both, energy and environmental applications. *Mater. Res. Bull.* **74**, 478 (2016).
45. H.W. Huang, K. Liu, K. Chen, Y.L. Zhang, Y.H. Zhang, and S.C. Wang: Ce and F comodification on the crystal structure and enhanced photocatalytic activity of Bi_2WO_6 photocatalyst under visible light irradiation. *J. Phys. Chem. C* **118**, 14379 (2014).
46. X.G. Han, Q. Kuang, M.S. Jin, Z. Xie, and L. Zheng: Synthesis of titania nanosheets with a high percentage of exposed (001) facets and related photocatalytic properties. *J. Am. Chem. Soc.* **131**, 3152 (2009).
47. Z.Y. Wang, K.L. Lv, G.H. Wang, K. Deng, and D. Tang: Study on the shape control and photocatalytic activity of high-energy anatase titania. *Appl. Catal., B* **100**, 378 (2011).
48. Y. Liu, L. Tian, X. Tan, X. Li, and X. Chen: Synthesis, properties, and applications of black titanium dioxide nanomaterials. *Sci. Bull.* **62**, 431 (2017).
49. F. Li, T. Han, H. Wang, X. Zheng, J. Wan, and B. Ni: Morphology evolution and visible light driven photocatalysis study of Ti^{3+} self-doped TiO_{2-x} nanocrystals. *J. Mater. Res.* **32**, 1563 (2017).
50. S. Shet, K. Ahn, T. Deutsch, H.L. Wang, N. Ravindra, Y.F. Yan, J. Turner, and M. Al-Jassim: Synthesis and characterization of band gap-reduced ZnO:N and ZnO:(Al,N) films for photoelectrochemical water splitting. *J. Mater. Res.* **25**, 69 (2010).
51. J. Prochazka, L. Kavan, M. Zukalova, P. Janda, J. Jirkovsky, Z.V. Zivcova, A. Poruba, M. Bedu, M. Döbbelin, and R. Tena-Zaera: Dense TiO_2 films grown by sol–gel dip coating on glass, F-doped SnO_2, and silicon substrates. *J. Mater. Res.* **28**, 385 (2013).
52. J. Wen, X. Li, W. Liu, Y. Fang, J. Xie, and Y. Xu: Photocatalysis fundamentals and surface modification of TiO_2 nanomaterials. *Chin. J. Catal.* **36**, 2049 (2015).
53. K.I. Ishibashi, A. Fujishima, T. Watanabe, and K. Hashimoto: Detection of active oxidative species in TiO_2 photocatalysis using the fluorescence technique. *Electrochem. Commun.* **2**, 207 (2000).
54. J. Zhu, S. Wang, Z. Bian, S. Xie, C. Cai, J. Wang, H. Yang, and H. Li: Solvothermally controllable synthesis of anatase TiO_2 nanocrystals with dominant {001} facets and enhanced photocatalytic activity. *CrystEngComm* **12**, 2219 (2010).
55. J.G. Yu, G.P. Dai, Q.J. Xiang, and M. Jaroniec: Fabrication and enhanced visible-light photocatalytic activity of carbon self-doped TiO_2 sheets with exposed {001} facets. *J. Mater. Chem.* **21**, 1049 (2011).
56. H.W. Huang, R.R. Cao, S. Yu, K. Xu, W. Hao, Y. Wang, F. Dong, T. Zhang, and Y.H. Zhang: Single-unit-cell layer established Bi_2WO_6 3D hierarchical architectures: Efficient adsorption, photocatalysis and dye-sensitized photoelectrochemical performance. *Appl. Catal. B Environ.* **219**, 526 (2017).
57. H.W. Huang, K. Xiao, T. Zhang, F. Dong, and Y.H. Zhang: Rational design on 3D hierarchical bismuth oxyiodides via in situ self-template phase transformation and phase-junction construction for optimizing photocatalysis against diverse contaminants. *Appl. Catal. B Environ.* **203**, 879 (2017).
58. J. Xie, L. Bian, L. Yao, Y.J. Hao, and Y. Wei: Simple fabrication of mesoporous TiO_2 microspheres for photocatalytic degradation of pentachlorophenol. *Mater. Lett.* **91**, 213 (2013).
59. H.W. Huang, X. Han, X. Li, S. Wang, P.K. Chu, and Y.H. Zhang: Fabrication of multiple heterojunctions with tunable visible-light-active photocatalytic reactivity in BiOBr–BiOI full-range composites based on microstructure modulation and band structures. *ACS Appl. Mater. Interfaces* **7**, 482 (2015).
60. K. Selvam, S. Balachandran, R. Velmurugan, and M. Swaminathan: Mesoporous nitrogen doped nano titania—A green photocatalyst for the effective reductive cleavage of azoxy benzenes to amines or 2-phenyl indazoles in methanol. *Appl. Catal., A* **413**, 213 (2012).
61. Y. Yan, T. Chen, Y. Zou, and Y. Wang: Biotemplated synthesis of Au loaded Sn-doped TiO_2 hierarchical nanorods using nanocrystalline cellulose and their applications in photocatalysis. *J. Mater. Res.* **31**, 1383 (2016).
62. K. Qi, B. Cheng, J. Yu, and W. Ho: A review on TiO_2-based *Z*-scheme photocatalysts. *Chin. J. Catal.* **38**, 1936 (2017).
63. C.D. Valentin, E. Finazzi, and G. Pacchioni: Density functional theory and electron paramagnetic resonance study on the effect of N-F codoping of TiO_2. *Chem. Mater.* **20**, 3706 (2008).
64. H.W. Huang, K. Xiao, N. Tian, F. Dong, T. Zhang, X. Du, and Y.H. Zhang: Template-free precursor-surface-etching route to porous, thin g-C_3N_4 nanosheets for enhancing photocatalytic reduction and oxidation activity. *J. Mater. Chem. A* **5**, 17452 (2017).
65. F. Wu, X. Li, W. Liu, and S. Zhang: Highly enhanced photocatalytic degradation of methylene blue over the indirect all-solid-state *Z*-scheme g-C_3N_4–RGO–TiO_2 nanoheterojunctions. *Appl. Surf. Sci.* **405**, 60 (2017).
66. X. Li, T. Xia, C. Xu, J. Murowchick, and X. Chen: Synthesis and photoactivity of nanostructured CdS–TiO_2 composite catalysts. *Catal. Today* **225**, 64 (2014).
67. F. Wu, W. Liu, J. Qiu, J. Li, W. Zhou, Y. Fang, S. Zhang, and X. Li: Enhanced photocatalytic degradation and adsorption of methylene blue via TiO_2 nanocrystals supported on graphene-like bamboo charcoal. *Appl. Surf. Sci.* **358**, 425 (2015).
68. H.W. Huang, Y. He, Z. Lin, L. Kang, and Y.H. Zhang: Two novel Bi-based borate photocatalysts: Crystal structure, electronic structure, photoelectrochemical properties, and photocatalytic activity under simulated solar light irradiation. *J. Phys. Chem. C* **117**, 22986 (2013).
69. H.W. Huang, S.C. Tu, C. Zeng, T. Zhang, A.H. Reshak, and Y.H. Zhang: Macroscopic polarization enhancement promoting photo- and piezoelectric-induced charge separation and molecular oxygen activation. *Angew. Chem., Int. Ed.* **56**, 11860 (2017).
70. L. Tian, J. Xu, A. Alnafisah, R. Wang, X. Tan, N.A. Oyler, L. Liu, and X. Chen: A novel green TiO_2 photocatalyst with a surface charge-transfer complex of Ti and hydrazine groups. *Chem. Eur. J.* **23**, 5345 (2017).
71. F. Liu, X. Yan, X. Chen, L. Tian, Q. Xia, and X. Chen: Mesoporous TiO_2 nanoparticles terminated with carbonate-like groups: Amorphous/crystalline structure and visible-light photocatalytic activity. *Catal. Today* **264**, 243 (2016).
72. L. Liu and X. Chen: Titanium dioxide nanomaterials: Self-structural modifications. *Chem. Rev.* **114**, 9890 (2014).
73. J.Y. Cheng, J. Chen, W. Lin, Y.D. Liu, and Y. Kong: Improved visible light photocatalytic activity of fluorine and nitrogen

co-doped TiO_2 with tunable nanoparticle size. *Appl. Surf. Sci.* **332**, 573 (2015).
74. J.L. Zhang, Y.M. Wu, M.Y. Xing, S.A.K. Leghari, and S. Sajjad: Development of modified N doped TiO_2 photocatalyst with metals, nonmetals and metal oxides. *Energy Environ. Sci.* **3**, 715 (2010).
75. X. Li, H.L. Liu, D.L. Luo, J.T. Li, Y. Huang, H.L. Li, Y.P. Fang, Y.H. Xu, and L. Zhu: Adsorption of CO_2 on heterostructure CdS (Bi_2S_3)/TiO_2 nanotube photocatalysts and their photocatalytic activities in the reduction of CO_2 to methanol under visible light irradiation. *Chem. Eng. J.* **180**, 151 (2012).

Supplementary Material

To view supplementary material for this article, please visit https://doi.org/10.1557/jmr.2018.106.